Improved registration for 3D image creation using multiple texel images and incorporating low-cost GPS/INS measurements

Scott E. Budge, Xuan Xie

Center for Advanced Imaging Ladar, Utah State University,
Logan, UT 84322-4120, (435) 797-3433

ABSTRACT

The creation of 3D imagery is an important topic in remote sensing. Several methods have been developed to create 3D images from fused ladar and digital images, known as texel images. These methods have the advantage of using both the 3D ladar information and the 2D digital imagery directly, since texel images are fused during data acquisition. A weakness of these methods is that they are dependent on correlating feature points in the digital images. This can be difficult when image perspectives are significantly different, leading to low correlation values between matching feature points.

This paper presents a method to improve the quality of 3D images created using existing approaches that register multiple texel images. The proposed method incorporates relatively low accuracy measurements of the position and attitude of the texel camera from a low-cost GPS/INS into the registration process. This information can improve the accuracy and robustness of the registered texel images over methods based on point-cloud merging or image registration alone. In addition, the dependence on feature point correlation is eliminated. Examples illustrate the value of this method for significant image perspective differences.

Keywords: lidar, ladar, 3D image creation, texel image, image registration, image and ladar fusion, point-cloud matching

1. INTRODUCTION

The production of 3D imagery is of interest in many applications, including watershed management, disaster management, documentation of historical sites, and digital elevation maps. On a smaller scale, 3D images can be used for object recognition in defense and surveillance applications such as targeting, monitoring, or person identification. In many of these applications, production of 3D images in real-time is desirable, as are methods that are robust to lighting, perspective differences in acquisition, and sensor noise.

A common method to produce 3D images is based in exploitation of stereo pairs by using the mathematics of projective geometry to triangulate 3D points from disparities in multiple images.[1–3] Although often effective, these methods are not robust in some practical situations. In addition, a significant amount of computation is required to construct the 3D surface. A good tutorial on image registration is given by Zitova and Flusser.[4]

For these reasons, direct sensing of a 3D surface using ladar imaging can be used to create a triangulated interconnected network (TIN or wireframe model) to represent the surface. This surface can then be textured with a digital (electro-optic or EO) image of the surface, creating a "texel image."[5] The sensors used to acquire texel images are designed to capture both the 3D measurements from a ladar and the EO imagery from a camera simultaneously. The texel image is therefore a fused dataset, where the 3D points are fused to the EO image at a sub-pixel level, and the spatial resolution of the image pixels is higher than the resolution of the ladar sensor. An additional advantage of these datasets is that there is no misregistration due to sensor motion.

Texel images are acquired from a single point of view, and therefore provide only a 2.5D representation of the object. To create a true 3D picture, it is necessary to register several texel images from different perspectives. The fused property of the texel image allows registration by stereo image techniques, 3D point cloud registration,[6–8] or both.[9]

This paper presents enhancements to the algorithm proposed by Budge and Badamikar[9] which incorporate coarse position and attitude information to improve the robustness and decrease the computation required to

Algorithm 1 Registration of texel images.

1. Detect Harris features.
2. Determine putative correspondences by 2D image correlation around features.
3. RANSAC using a fundamental matrix model and the epipolar constraint.
4. Estimate the optimal fundamental matrix and determine putative correspondences that meet both the correlation threshold and the epipolar constraint.
5. Match point clouds using fused EO image/lidar data to create an estimate of the registration transformation $(\hat{\boldsymbol{R}}, \hat{\boldsymbol{t}})$.
6. Use the current estimate $(\hat{\boldsymbol{R}}, \hat{\boldsymbol{t}})$ and the fused EO image/lidar data to test putative correspondences and eliminate bad ones:
   (a) Find the 3D points $\boldsymbol{x}_i$ in image 1 corresponding to the set of possible putative correspondences ($\boldsymbol{u}_i$,$\boldsymbol{u'}$).
   (b) Transform the 3D points to the coordinate system of image 2 using $(\hat{\boldsymbol{R}}^T, -\hat{\boldsymbol{t}})$, creating the set $\hat{\boldsymbol{x}}'_i$.
   (c) Project the $\hat{\boldsymbol{x}}'_i$ into image 2, creating $\hat{\boldsymbol{u}}'_i$.
   (d) Select the feature point out of the $\hat{\boldsymbol{u}}'_i$ that is closest to $\boldsymbol{u'}$ in image 2. Discard the rest of the set.
   (e) The 2D distance between the selected feature point and $\boldsymbol{u'}$ must be below a threshold. Otherwise, the set of correspondences $(\boldsymbol{u}_i, \boldsymbol{u'})$ is removed.
7. Repeat step 5.

accurately register texel images. If high-quality position and attitude information is available in a common reference frame, no registration is needed. However, low-cost systems are much less accurate, and registration must be used to produce high-quality 3D images.

The remainder of the paper proceeds as follows. Section 2 begins by reviewing a previous registration method and describing the difficulties associated with correlation-based methods. Section 3 describes the algorithm used to register the datasets using coarse position and attitude information. Registration results are given in Section 4, and Section 5 concludes the paper.

2. CORRELATION-BASED REGISTRATION OF TEXEL IMAGES

In a previous work, an algorithm was proposed that successfully registers texel images when no *a priori* information about the position and attitude of the texel camera is known.[9] It takes advantage of both the EO data and the point cloud data in texel images, and requires that there be overlap in the images that contains a set of corresponding feature points $(\boldsymbol{u}, \boldsymbol{u'})$, where $\boldsymbol{u}$ is a point in the first image, and $\boldsymbol{u'}$ is a point in the second image. Algorithm 1 summarizes the steps for registering texel images acquired from arbitrary overlapping perspectives. The end result of the algorithm is an estimate of the 3D rotation matrix, $\hat{\boldsymbol{R}}$, and translation vector, $\hat{\boldsymbol{t}}$, between the first texel image and the second texel image.

The method is limited in performance by a characteristic common to algorithms that rely on finding feature point correspondences in images using correlation. When the perspectives are widely separated, perspective distortion in the images causes the correlation between true correspondences to decrease to the point where correlation thresholds are not robust. An example of this problem is given in Figure 1, where a potential Harris feature point is circled in green. Figure 1 (a) is from a perspective in front of a checkered cube, and Figure 1 (b) is from above. It is evident that the image pixels around the point are significantly different, and will lead to a low correlation value.

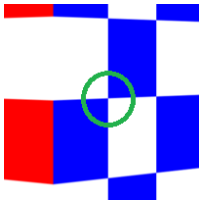

(a) Front perspective.

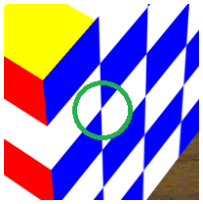

(b) Top perspective.

Figure 1: Examples of potential Harris feature points on a checkered cube from different perspectives.

Several authors have proposed methods to address this problem in matching feature points in imagery. These methods can be generally classed as affine-invariant methods,[10,11] scale-invariant methods,[12,13] or other feature-based methods.[14,15]

A second disadvantage of correlation-based methods is the computational cost. Correlation is performed using a window of image pixels around each feature point. Every point in the first image is correlated with every point in the second image, and a list of putative correspondences is created where the correlation value between points exceeds a threshold. This list may be many-to-one, where multiple points in one image correlate with a point in the other image. For a list of N_1 features in the first image, N_2 features in the second image, and $N_2 \geq N_1$, the total number of correlations that must be performed is $N_1(N_2 - N_1/2 + 1/2)$, or order $\mathcal{O}(N_1 N_2)$.

3. TEXEL IMAGE REGISTRATION USING COARSE POSITION AND POSE INFORMATION

Registration of texel images taken from multiple perspectives is trivial when highly accurate position and attitude information is known, and can be acquired using high-cost, state-of-the-art differential global positioning systems (GPS) and inertial navigation units (IMU). The goal of this work is to propose a method to register texel images using coarse GPS/IMU information available from small, low-cost microelectromechanical systems (MEMS). These GPS/IMU sensors can be integrated with a miniaturized texel camera and used in a small unmanned aerial system (UAS) for a cost low enough to make the UAS accessible to a wide range of users.

In addition, as described in Section 2, it is desirable to remove the dependence of the registration on image correlation. The unique properties of texel images allow exploitation of both the EO image and the point cloud in the fused dataset to determine if feature points are putative correspondences. Image correlation around feature points appears in Algorithm 1 in steps 2 and 4. Coarse GPS/IMU information will be used to replace the need for correlation in these steps of the algorithm as follows.

The EO image is exploited using the fact that putative correspondences in images from different perspectives must meet the epipolar constraint,[2] which states that if $\boldsymbol{u}$ and $\boldsymbol{u}'$ are corresponding (homogeneous) points in image 1 and image 2 which are projected from a single 3D point $\boldsymbol{x}$ visible in both images, and $\boldsymbol{F}$ is the fundamental matrix for the image pair, the constraint

$$\boldsymbol{u'}^T \boldsymbol{F} \boldsymbol{u} = 0 \tag{1}$$

must hold. Assuming an estimate is available for the rotation matrix and translation vector between texel image 1 and texel image 2, $(\hat{\boldsymbol{R}}, \hat{\boldsymbol{t}})$, the fundamental matrix can be estimated using

$$\hat{\boldsymbol{F}} = \boldsymbol{K}^{-T} [\hat{\boldsymbol{t}}_\times] \hat{\boldsymbol{R}} \boldsymbol{K}^{-1}, \tag{2}$$

where $\boldsymbol{K}$ is the EO camera calibration matrix (intrinsic parameters), and

$$[\hat{\boldsymbol{t}}_\times] = \begin{bmatrix} 0 & -\hat{z}_t & \hat{y}_t \\ \hat{z}_t & 0 & -\hat{x}_t \\ -\hat{y}_t & \hat{x}_t & 0 \end{bmatrix} \tag{3}$$

(constructed from $\hat{\boldsymbol{t}} = \begin{bmatrix} \hat{x}_t & \hat{y}_t & \hat{z}_t \end{bmatrix}^T$).

The point cloud (3D) information in the texel images is used to create a second restriction on putative correspondences. Each EO image feature $\boldsymbol{u}$ has a corresponding 3D point $\boldsymbol{x}$ (either through direct measurement or interpolation of surrounding 3D measurements). The 3D point $\boldsymbol{x'}$ corresponding to the feature $\boldsymbol{u'}$ in texel image image 2 can be transformed into the coordinate system of texel image 1 using the relationship

$$\hat{\boldsymbol{x}} = \begin{bmatrix} \hat{x} & \hat{y} & \hat{z} \end{bmatrix}^T = \begin{bmatrix} \hat{\boldsymbol{R}} & \hat{\boldsymbol{t}} \end{bmatrix} \begin{bmatrix} \boldsymbol{x'} \\ 1 \end{bmatrix}. \tag{4}$$

If $(\hat{\boldsymbol{R}}, \hat{\boldsymbol{t}})$ are noiseless, then $\boldsymbol{x} = \hat{\boldsymbol{x}}$. The estimates of $(\hat{\boldsymbol{R}}, \hat{\boldsymbol{t}})$ are given by a MEMS GPS/IMU, and are therefore in error, however, the pair $(\boldsymbol{x}, \hat{\boldsymbol{x}})$ should be close to each other in 3D space if $(\boldsymbol{u}, \boldsymbol{u'})$ are correct correspondences.

These two tests can then be used to replace the correlation in Algorithm 1. First, the fundamental matrix is computed using (2) and the MEMS GPS/IMU measurement. All feature points found in the first image are tested against all points in the second image to determine if $\boldsymbol{u'}^T \hat{\boldsymbol{F}} \boldsymbol{u}$ is below a threshold. For each potential pair that passes the test, the corresponding 3D points are compared to determine if the distance between them is below a threshold. If true, the pair is added to the list of putative correspondences.

The previous step can be repeated by computing the rigid transformation $(\hat{\boldsymbol{R}}, \hat{\boldsymbol{t}})$ from the 3D correspondences,[16] using these to compute the fundamental matrix, and decreasing the thresholds each iteration. This has the effect of removing more incorrect correspondences as the thresholds get smaller. At this point in the algorithm, all of the point correspondences that meet the two tests are kept, which can result in a many-to-one mapping between point correspondences. This is denoted as the set $(\boldsymbol{u}, \hat{\boldsymbol{u}}_i')$, where there are i features in image 2 that correspond to a feature in image 1.

The tests can also replace step 6 in Algorithm 1, with a slight modification. At this step, the goal is to find best correspondence between a point in one image and a point in the other. Any many-to-one correspondences are eliminated by choosing the pair $(\boldsymbol{u}, \boldsymbol{u'})$ associated with pair $(\boldsymbol{x}, \hat{\boldsymbol{x}})$ with the smallest distance. If the smallest distance is above a threshold, the entire set $(\boldsymbol{u}, \hat{\boldsymbol{u}}_i')$ is discarded. The final algorithm is given in Algorithm 2. Details for steps 6–8 are given by Budge and Badamikar.[9]

The RANSAC[17] step was retained from Algorithm 1 because the points are eliminated using a different mechanism than in steps 2–5. The fundamental matrix is selected that fits the most data, instead of the matrix that is computed from $(\hat{\boldsymbol{R}}, \hat{\boldsymbol{t}})$. It was observed that RANSAC runs with many fewer iterations than in Algorithm 1 due to the epipolar test used in prior steps.

4. REGISTRATION RESULTS

The registration method given in Algorithm 2 was tested using three types of datasets. First, synthetic texel images were created using 3D models and textures from digital images. These were used to test for performance of the algorithm when the attitude and position of the two texel images is known, and errors are introduced in the attitude and position of one image.

After convergence was tested on these synthetic images, images of a similar scene were taken with a texel camera. The real images contain significant noise in the 3D measurements, and the attitude and position of the camera for each texel image was measured with an accuracy of about 5 mm in position and a few degrees in attitude. Both the synthetic and real scenes were constructed with objects textured with potential for finding many Harris features. Although this is artificial, it enables confirmation of the basic theory without failure due to a lack of available features. Examples of the texel images for both datasets are given in Figure 2, where 2 (c) illustrates the error in registration when $(\hat{\boldsymbol{R}}, \hat{\boldsymbol{t}})$ contains errors. Note that the blocks show an offset, and the background map is shifted. Finally, tests were conducted with a more natural scene.

Algorithm 2 Improved registration of texel images using position and attitude estimates.

1. Detect Harris features.
2. Compute the fundamental matrix $\hat{\boldsymbol{F}}$ using (2).
3. Determine putative correspondences using $\hat{\boldsymbol{F}}$ and the position and attitude information $(\hat{\boldsymbol{R}}, \hat{\boldsymbol{t}})$:
   (a) Test each potential correspondence to determine that $\boldsymbol{u'}^T \hat{\boldsymbol{F}} \boldsymbol{u}$ is below a threshold.
   (b) If true, test that the distance between the corresponding 3D points $(\boldsymbol{x}, \hat{\boldsymbol{x}})$ is below a threshold.
4. Match point clouds using fused EO image/lidar data to create an estimate of the registration transformation $(\hat{\boldsymbol{R}}, \hat{\boldsymbol{t}})$.
5. Repeat steps 2–4 a fixed number of times, decreasing the thresholds each iteration.
6. RANSAC using a fundamental matrix model and the epipolar constraint.
7. Estimate the optimal fundamental matrix $\hat{\boldsymbol{F}}$ and determine putative correspondences that meet the epipolar constraint to within a threshold.
8. Match point clouds using fused EO image/lidar data to create an estimate of the registration transformation $(\hat{\boldsymbol{R}}, \hat{\boldsymbol{t}})$.
9. Use the current estimate $(\hat{\boldsymbol{R}}, \hat{\boldsymbol{t}})$ and the fused EO image/lidar data to test putative correspondences and eliminate incorrect and many-to-one correspondences:
   (a) Test each potential correspondence to determine that $\boldsymbol{u'}_i^T \hat{\boldsymbol{F}} \boldsymbol{u}$ is below a threshold.
   (b) If true, test that the distance between the corresponding 3D points $(\boldsymbol{x}, \hat{\boldsymbol{x}}_i)$ is below a threshold. If all i in the set have a distance greater than the threshold, discard the set $(\boldsymbol{u}, \hat{\boldsymbol{u}}'_i)$.
   (c) Select the correspondence with the minimum distance out of the set of i correspondences.
10. Repeat step 8.

(a) Simulated texel image. (b) Real texel image. (c) Real texel images with registration mismatch.

Figure 2: Examples of synthetic and real texel images.

4.1 Algorithm Convergence

The convergence of the algorithm was tested by creating two synthetic texel images with a known attitude and position transformation $(\boldsymbol{R}, \boldsymbol{t})$ from one to the other. Several shifts in $\boldsymbol{t}$ in the range of 0-5 cm, and rotations in $\boldsymbol{R}$ from 0-5° were added to the true values to create an estimate $(\hat{\boldsymbol{R}}, \hat{\boldsymbol{t}})$ containing a simulated MEMS GPS/IMU

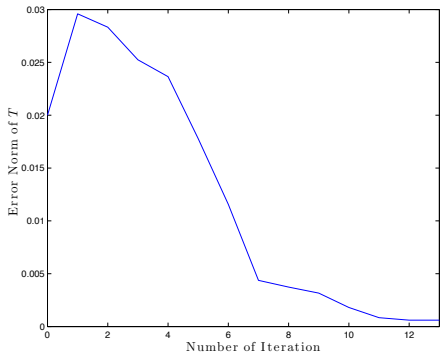

(a) Error in the estimate of $\hat{\boldsymbol{t}}$.

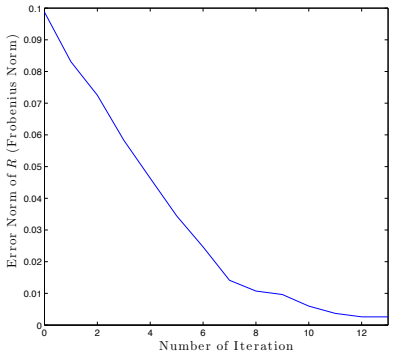

(b) Error in the estimate of $\hat{\boldsymbol{R}}$ measured using the Frobenious norm.

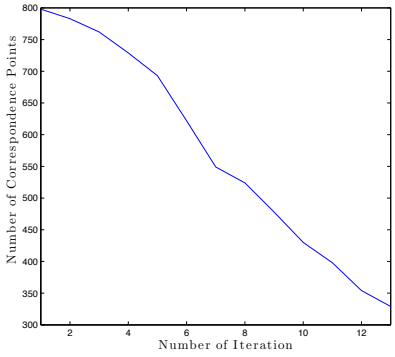

(c) Number of correspondences.

Figure 3: Convergence of steps 2–5 for the values of $\hat{\boldsymbol{t}}$, $\hat{\boldsymbol{R}}$, and the number of correspondences. The initial error was 2 cm in $\hat{\boldsymbol{t}}$, and a rotation error of 5°.

error. The scene had a maximum depth of about 1.5 m, so the translation represents a maximum 3D position distance error of about 3.3% due to translation error, and about 8.7% due to attitude error. To compare, a UAS flying at 300 m altitude using a typical MEMS GPS/IMU would experience a maximum translation error of about 5 m (1.7%) and maximum attitude error corresponding to about 10.5 m (3.5%, assuming a rotation error of 2°).

Several different combinations of translation and rotation errors in the range were tested, and all were found to result in convergence to the correct $(\boldsymbol{R}, \boldsymbol{t})$ within a small error by the start of step 6 in Algorithm 2. The initial threshold for the epipolar test was 0.05, the initial threshold for the distance test was 0.08, and the thresholds were decreased by 20% each iteration. An example of the convergence plots is given in Figure 3, where the initial error in $\hat{\boldsymbol{t}}$ is 2 cm, and the initial rotation error is 5°. Note that in Figure 3 (c), the number of correspondences decreases each iteration of steps 2–5 as the tests remove outliers.

4.2 Registration of Real Texel Images

The registration algorithm begins by detecting Harris features[18] in each of the EO images. Each of the color planes are processed individually, and the points from each of the planes are added to a list of feature points. An example of the features found in real texel images is given in Figure 4. In this example, the true image attitude and position differences were measured to be approximately a 9 cm shift up, a 15° downward rotation in elevation, and a 5° rotation counterclockwise in azimuth. The "noise" added to the measurement included a 2 cm shift and a 5° rotation. As seen in Figure 4. a number of the features occur at noisy points in the image which must be removed before accurate registration can occur.

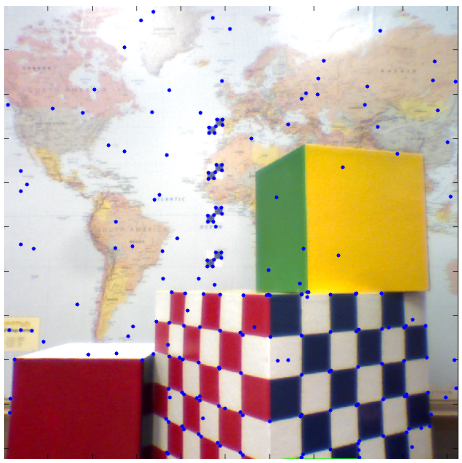

(a) Texel image 1

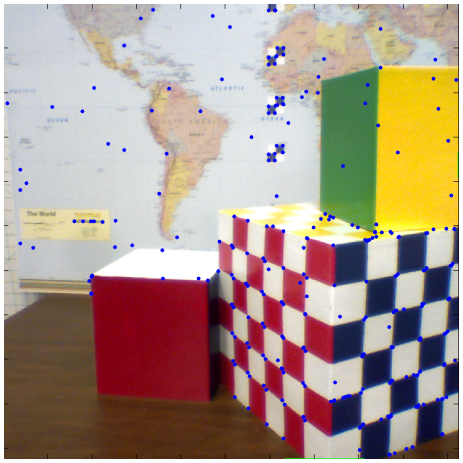

(b) Texel image 2

Figure 4: Examples of Harris features found in the texel images and marked with blue dots.

(a) Texel image 1

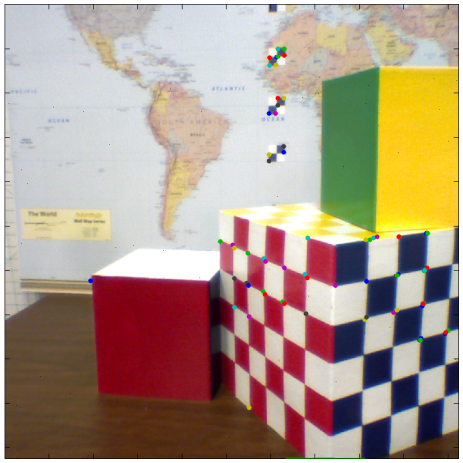

(b) Texel image 2

Figure 5: Examples of putative correspondences found using coarse position and attitude estimates without correlation. Colored dots mark correspondence pairs.

Once these features are found, the epipolar test and the distance test are executed (steps 2–5) on potential correspondences, without using correlation, and the putative correspondences are determined. The initial estimate of $\hat{\boldsymbol{F}}$ was computed using the noisy values of $(\hat{\boldsymbol{R}}, \hat{\boldsymbol{t}})$ described above. These putative correspondences are shown in Figure 5.

After the completion of the algorithm, the final putative correspondences are shown in Figure 6. In the Figure, the white lines are the epipolar lines that each surviving correspondence lies on. Note that the surviving correspondences are good matches and are located in different parts of the texel image. These are then used to compute the final estimate of $(\hat{\boldsymbol{R}}, \hat{\boldsymbol{t}})$. From these, the texel images can be registered as shown in Figure 7.

Figure 8 illustrates the performance of the algorithm on a more natural scene. In this experiment, the position and attitude of the texel images was approximately known, and a translation error of 3 cm and rotation error of 3° was added. Note that there are undetermined errors in the initial measurement of $(\hat{\boldsymbol{R}}, \hat{\boldsymbol{t}})$; the actual errors are larger than a 3 cm shift and a 3° rotation. The results show that registration without correlation can be successful with typical position and attitude errors.

(a) Texel image 1

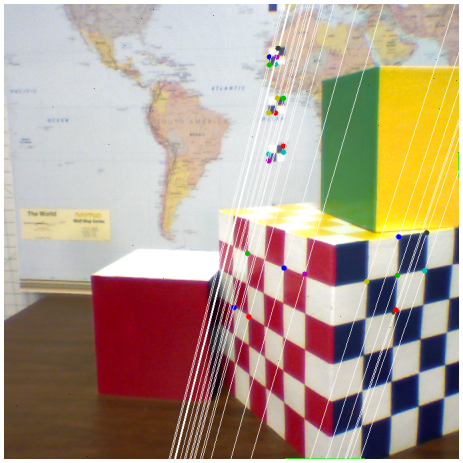

(b) Texel image 2

Figure 6: Examples of final putative correspondences. Colored dots mark correspondence pairs. The white lines are epilines.

(a) Registered simulated texel images.

(b) Registered real texel images.

Figure 7: Final registration results. All images are taken from a 3D viewing program.

5. CONCLUSION

The method described in this paper has shown to perform very well in registering textured 3D point clouds (texel images) with coarse knowledge of the position and attitude of the camera and without the need for correlation. This can make the algorithm more robust in the cases in which the images are taken from wide perspectives, where the projective nature of cameras distorts images so that the pixels around feature points do not exhibit high correlation. In addition, the run time before step 6 in Algorithm 2 was observed to be significantly shorter. This makes the heavy computational cost of correlation and invariant transforms on feature points unnecessary.

Coarse position and attitude information can be available for a small, low-cost UAS by using one of the many available MEMS GPS/IMU systems. These systems are also low cost, but have the disadvantage of much higher attitude error than the state-of-the-art IMU systems. The registration algorithm proposed here can produce good results even when presented with errors in position and attitude.

Registration is based on the unique properties of texel images, which contain both 2D and 3D information about a scene. Registration creating 3D images using significantly lower computation can be performed because the images must satisfy both the properties of projective geometry and 3D rigid transformation.

(a) Texel image 1 (b) Texel image 2. (c) Registered texel images.

Figure 8: Example of image registration on a more natural scene.

REFERENCES

[1] Scharstein, D. and Szeliski, R., "A taxonomy and evaluation of dense two-frame stereo correspondence algorithms," *Int. J. of Comp. Vision* **47**, 7–42 (Apr. 2002).

[2] Hartley, R. and Zisserman, A., [*Multiple View Geometry in Computer Vision*], Cambridge University Press, second ed. (2003).

[3] Remondino, F., El-Hakim, S. F., Grün, A., and Zhang, L., "Turning images into 3-D models," *IEEE Signal Process. Mag.* **25**, 55–65 (July 2008).

[4] Zitova, B. and Flusser, J., "Image registration methods: a survey," *Image Vis. Comput.* **21**, 977–1000 (Oct. 2003).

[5] Budge, S. E. and Badamikar, N. S., "Calibration method for texel images created from fused lidar and digital camera images," *Opt. Eng.* **52**, 103101 (Oct. 2013).

[6] Besl, P. J. and McKay, N. D., "A method for registration of 3-D shapes," *IEEE Trans. Pattern Anal. Mach. Intell.* **14**, 239–256 (Feb. 1992).

[7] Rusinkiewicz, S. and Levoy, M., "Efficient variants of the ICP algorithm," in [*Third International Conference on 3-D Digital Imaging and Modeling*], 145–152 (May–June 2001).

[8] Nishino, K. and Ikeuchi, K., "Robust simultaneous registration of multiple range images," in [*Proc. 5th Asian Conf. Computer Vision*], 454–461 (2002).

[9] Budge, S. E. and Badamikar, N., "Automatic registration of multiple texel images (fused lidar/digital imagery) for 3D image creation," in [*Laser Radar Technology and Applications XVIII*], Turner, M. D. and Kamerman, G. W., eds., **8731**, 873107, SPIE, Baltimore, Maryland, USA (June 2013).

[10] Baumberg, A., "Reliable feature matching across widely separated views," in [*Proc. IEEE Conf. Computer Vision and Pattern Recogition (CVPR)*], **1**, 774–781 (June 2000).

[11] Tuytelaars, T. and Van Gool, L., "Matching widely separated views based on affine invariant regions," *Int. J. of Computer Vision* **59**(1), 61–85 (2004).

[12] Brown, M. and Lowe, D. G., "Automatic panoramic image stitching using invariant features," *Int. J. of Computer Vision* **74**(1), 59–73 (2007).

[13] Lindeberg, T., "Scale selection properties of generalized scale-space interest point detectors," *J. of Math. Imaging and Vision* **46**(2), 177–210 (2013).

[14] Yasein, M. S. and Agathoklis, P., "A robust, feature-based algorithm for aerial image registration," in [*IEEE Int. Sym. on Industrial Elect.*], 1731–1736 (June 2007).

[15] Liang, J. and Zhou, Y., "Vector features for image matching and image registration," in [*Fifth Int. Conf. on Graphic and Image Proc. (ICGIP 2013)*], **9069**, 906918 (2014).

[16] Eggert, D. W., Lorusso, A., and Fisher, R. B., "Estimating 3-D rigid body transformations: a comparison of four major algorithms," *Machine Vision and Applications* **9**(5/6), 272–290 (1997).

[17] Fischler, M. A. and Bolles, R. C., "Random sample consensus: a paradigm for model fitting with applications to image analysis and automated cartography," *Comm. ACM* **24**, 381–395 (June 1981).

[18] Harris, C. and Stephens, M., "A combined corner and edge detector," in [*In Proc. of Fourth Alvey Vision Conf.*], 147–151 (1988).